Title

Vertical meteorological patterns and their impact on the energy demand of tall buildings

Authors

Gui, Chenxi

Yan, Da

Hong, Tianzhen

et al.

Publication Date

2021-02-01

DOI

10.1016/j.enbuild.2020.110624

Peer reviewed

Building Technologies & Urban Systems Division
Energy Technologies Area
Lawrence Berkeley National Laboratory

Vertical Meteorological Patterns and their Impact on the Energy Demand of Tall Buildings

Chenxi Gui[1], Da Yan[1], Tianzhen Hong[2], Chan Xiao[3], Siyue Guo[1,4], Yifan Tao[5]

[1]School of Architecture, Tsinghua University, Beijing, China
[2]Building Technology and Urban Systems Division, Lawrence Berkeley National Laboratory, Berkeley, USA
[3]National Climate Center, China Meteorological Administration, Beijing, China
[4]Institute for Energy, Environment & Economy, Tsinghua University, Beijing, China
[5]Institute of Atmospheric Physics, Chinese Academy of Science, Beijing, China

Energy Technologies Area
February 2021

DOI: 10.1016/j.enbuild.2020.110624

This work was supported by the Assistant Secretary for Energy Efficiency and Renewable Energy, Building Technologies Office, of the U.S. Department of Energy under Contract No. DE-AC02-05CH11231.

Vertical Meteorological Patterns and their Impact on the Energy Demand of Tall Buildings

Chenxi Gui [1], Da Yan [1,*], Tianzhen Hong [2,*], Chan Xiao [3], Siyue Guo [1,4], Yifan Tao [5]

[1] School of Architecture, Tsinghua University, Beijing, China

[2] Building Technology and Urban Systems Division, Lawrence Berkeley National Laboratory, Berkeley, USA

[3] National Climate Center, China Meteorological Administration, Beijing, China

[4] Institute for Energy, Environment & Economy, Tsinghua University, Beijing, China

[5] Institute of Atmospheric Physics, Chinese Academy of Science, Beijing, China

*Corresponding authors. E-mail address: yanda@tsinghua.edu.cn (Da Yan), thong@lbl.gov (Tianzhen Hong)

Abstract

In accordance with the developing economy and growing population, an increasing number of tall buildings have been constructed over the last 20 years. In 2017, there were 144 new buildings worldwide that were 200 m or greater in height; 50% of these buildings were in China. Due to the vertical gradient impact of meteorological parameters, the energy performance of tall buildings differs from that of general buildings. Few studies exist on vertical meteorological changes using measured data at different heights. Most studies on dynamic energy simulation simulate meteorological parameters using models. This study explores vertical meteorological patterns using hourly dry-bulb temperature, relative humidity, and wind speed data from 2007 to 2017 for a 325 m meteorological tower in Beijing. The temperature decreased significantly with increasing altitude (~0.9 °C per 100 m), while the daily temperature difference decreased with increasing altitude. The absolute humidity did not change significantly with height. The wind speed increased with altitude at approximately 2 m/s per 100 m. The building simulation showed that the annual heating load at a height of 320 m increased by 85% from that at 8 m; the annual cooling load decreased by 20%. Such significant differences in thermal loads for 300-m-tall buildings confirm the need to consider vertical meteorological differences in building performance simulations for tall buildings. A greater number of measurement points at different heights improve the simulation accuracy. Guidance on selecting the heights for vertical metrological measurements is provided based on the influences of building thermal loads.

Keywords: meteorological towers; building energy demands; microclimates; vertical meteorological patterns; weather parameters, tall buildings

1 Introduction

Rapid economic development and population growth have caused an increase in the

number of tall buildings constructed over the last 20 years. The number of newly constructed buildings is shown in Figure 1. The Council on Tall Buildings and Urban Habitat (CTBUH) defines tall buildings as those with a height greater than 50 m or consist of more than 14 storeys [1]. The national standard in China, GB 50352-2005 Uniform Standard for Design of Civil Buildings, classifies buildings according to their number of floors or height above the ground. The standard considers buildings greater than 100 m in height "super-tall buildings" [2].

According to the CTBUH [3], in 2017, there were 144 newly constructed buildings worldwide reaching 200 m or greater in height; 72 of these buildings were in China, accounting for 50% of the global total. As of January 2020, China had 2155 buildings over 150 m, 750 buildings over 200 m, and 84 buildings over 300 m. Based on these numbers, China ranks first in the world, as shown in Figure 2. Of the ten cities worldwide with the largest number of buildings over 150 m in height, cities in China account for approximately 60%. In Beijing, the number of tall buildings has grown rapidly. As of January 2020, there were 67 buildings greater than 100 m in height, approximately 97% of which were less than 300 m, and two new buildings that were over 300 m.

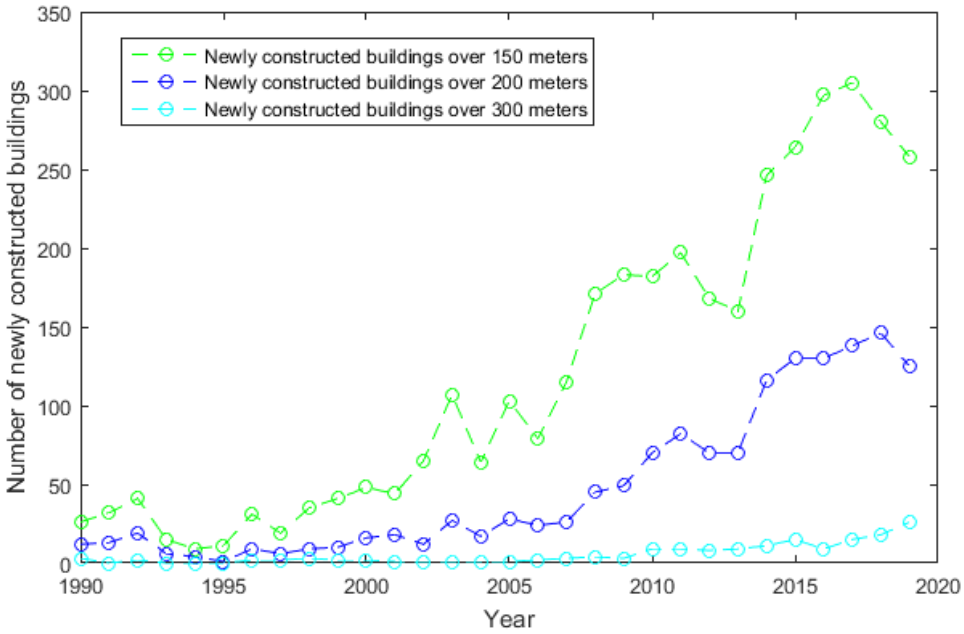

Figure 1 Number of newly constructed buildings in the world (1990–2019).

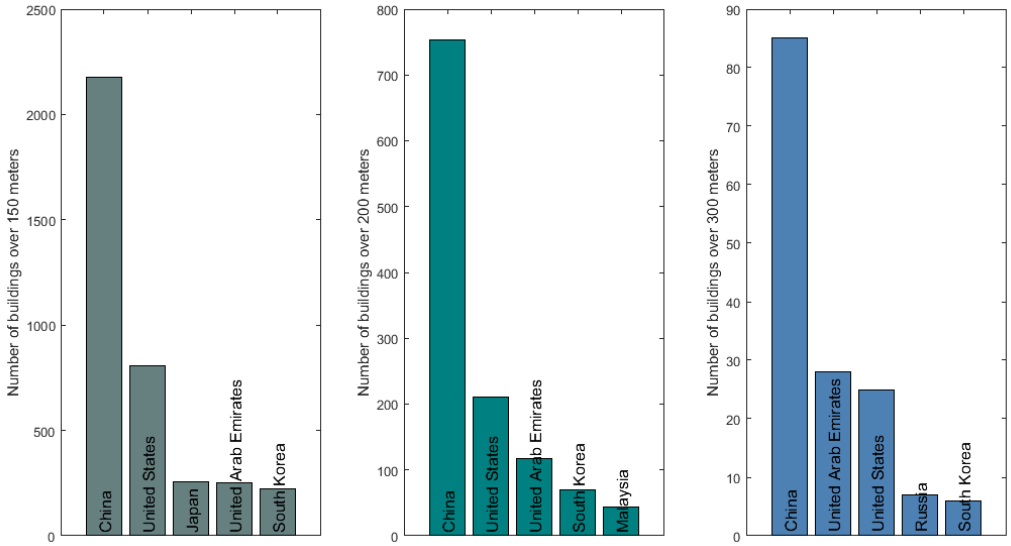

Figure 2 Countries ranked by number of completed tall buildings (as of March 2020).

With an increasing number of tall buildings, numerous simulation studies have been conducted to support tall-building design or evaluate energy performance. Building energy performance is affected by a variety of factors, including meteorological conditions, building envelope, indoor environmental parameters, occupant behavior, equipment and system type, and operational management [4]. Of these inputs, meteorological conditions need to be reconsidered for tall building simulations. Typically, only one set of meteorological parameters is inputted (e.g., typical-meteorological-year weather data) when the energy performance of a single building is simulated. These parameters are used to simulate the performance of all floors of a building without adjusting the meteorological parameters [5]. Wang et al. [6] discussed the effect of vertical variations in meteorological parameters. They calculated outdoor weather parameters used for building design at different heights and compared them to values of low-rise buildings, finding a difference of less than 0.5 °C. As such, it was concluded that outdoor weather parameters can be treated the same as the ground-level values for high-rise buildings less than 200 m in height. However, in tall buildings with height of 300 m or above, the meteorological parameters change at different heights, and these differences cannot be ignored.

There are previous studies on the vertical variations of meteorological parameters and their influences on simulated building performance results. Tong et al. [7] analyzed the natural ventilation potential at different heights for high-rise buildings in major cities across six climate zones in the United States (US), considering the diurnal cycle of the atmospheric boundary layer. They found that building height greatly influenced the vertical pattern of natural ventilation. The potential for utilizing NV strategies significantly depends on the local climate [8]. Jung et al. [9] considered the vertical weather profile to obtain a weather-delay simulation model and quantify how this influences building construction delay. Saroglou et al. [10] simulated two building models with different envelopes and heights in Tel Aviv, Israel. They considered the changing microclimate generated by the data measured by a meteorological station at different heights and equations representing vertical variations. Their results showed that the heating energy use of the residential tower increased by three

times for floors from 7.75 to 390.6 m. Sinha et al. [11] developed a theoretical model considering temperature and humidity affected by solar energy, atmospheric turbidity, and pollutants, and calculated the heating, ventilation, and air conditioning (HVAC) loads in Delhi, India. Their results showed a difference of 20% for an office building 200 m in height when compared to the results calculated from the data measured by the meteorological station. Segal et al. [12] analyzed the weather patterns of some US cities using radiosonde measured data to better calculate building loads. Song et al. [13, 14] used radiosonde measured data to calculate the heating and cooling loads of super-tall buildings in Osan, Korea. The observed parameters included outdoor air temperature, humidity, and wind speed. This study showed that the cooling load decreased by 27% and the heating load increased by 290% when vertical weather variations were considered for a 200-storey building. Cao [15] and Zhang [16] studied the vertical changes in outdoor environments in Dalian and Beijing based on the mesoscale meteorological model, Weather Research Forecast (WRF) [17]. They also explored the impact of heating and cooling loads at each vertical section of the building. Cao [15] found that the height and orientation of the rooms had a large effect on thermal loads. Ellis et al. [18] used EnergyPlus to simulate two tower models considering changes in outdoor air temperature and wind speed along the vertical direction. EnergyPlus [19] considers variations in meteorological parameters such as air temperature and wind speed with altitude, and users can input meteorological profiles for simulation. By changing these parameters, they found a significant effect on building energy use.

In general, most studies on the load characteristics of tall buildings are based on theoretical formulas or meteorological models to obtain meteorological data at different heights. With the development of meteorological observation methods and computing technology in recent years, the quantity and quality of meteorological data have greatly improved. Such data better reflect vertical meteorological variations under actual conditions. As such, if this data is used in building simulations, it has the capacity to improve the accuracy of simulated thermal loads for tall buildings.

In this study, we used an 11-year dataset of measurements from a 320 m meteorological tower in Beijing to investigate the following: (1) the vertical meteorological profile in Beijing, revealing the vertical patterns of meteorological parameters such as variations in dry-bulb temperature, absolute humidity, and wind speed at different heights and times under actual conditions; and (2) the influence of the vertical meteorological profile on building cooling and heating loads in Beijing.

2 Method

2.1 Data source

This study used 11 years of measured data (2007 to 2017) from a meteorological tower (herein referred as “the Tower”) in Beijing. The data included the outdoor dry-bulb temperature, absolute humidity, and wind speed measured at various heights. The Tower was built in 1979 and is located between the Third Ring Road and the Fourth Ring Road in Beijing. It is 325 m high and the base is 49 m above sea level [20]. The tower is located in an open space with minimal wind shielding from its surroundings. It has 15 observation platforms. A sketch of the

tower is shown in Figure 3. The figure illustrates that the tower is comprised of 15 observation platforms at various heights, all of which measure outdoor dry-bulb temperature, absolute humidity, and wind speed. There are some instances of data loss in the measured hourly meteorological data. The missing data includes dry-bulb temperature, relative humidity, and wind speed data, which have been calculated separately, as shown in Figure 4. In this figure, "Data missing rate" refers to the percentage of missing points in 8 760 h in each year. The missing data were lower between 2013 and 2016. There were several measurement gaps for relative humidity measured in some platforms from 2007 to 2012. The analysis of vertical meteorological patterns in this study was conducted based on a group of data for statistical analysis—for example, the study of vertical meteorological patterns based on data from multiple platforms at the same measured hour, or the study of daily range based on data from several measured hours on the same platform. Therefore, if there was data loss at a certain time or height in the dataset used for analysis, this set of data was removed from the basic data. This procedure was undertaken for relative humidity and dry-bulb temperature data. In addition, two other derived meteorological indices were calculated to reflect differences between weather data at various heights: heating degree-day (HDD) and cooling degree-day (CDD). In this study, an HDD18 (with 18 °C as the base temperature) and CDD26 (with 26 °C as the base temperature) were used based on the national standard in China: the JGJ26 – 2010 Design Standard for Energy Efficiency of Residential Buildings in Severe Cold and Cold Zones [21].

Other meteorological parameters used in the simulation were derived from the fifth-generation reanalysis meteorological data dataset (ERA5), including atmospheric pressure, solar radiation, ground temperature, and effective sky temperature. ERA5 is a reanalysis dataset of the European Center for Medium-Term Weather Forecasting (ECMWF) [22]. We downloaded hourly instantaneous weather variables at 39°54'N, 116°23'E from 2007 to 2017. This included surface pressure, total cloud cover, skin temperature, and the hourly accumulated data of surface solar radiation downward and the total sky direct solar radiation at the surface. The total cloud cover and skin temperature were used to generate the hourly effective sky temperature [23].

As the building load simulation required continuous time-series weather data as input parameters, the missing data were filled in via interpolation to generate continuous time-series data. In terms of data reliability, this part of the simulation study was mainly based on data from 2013 to 2016, when the rate of data loss was lower.

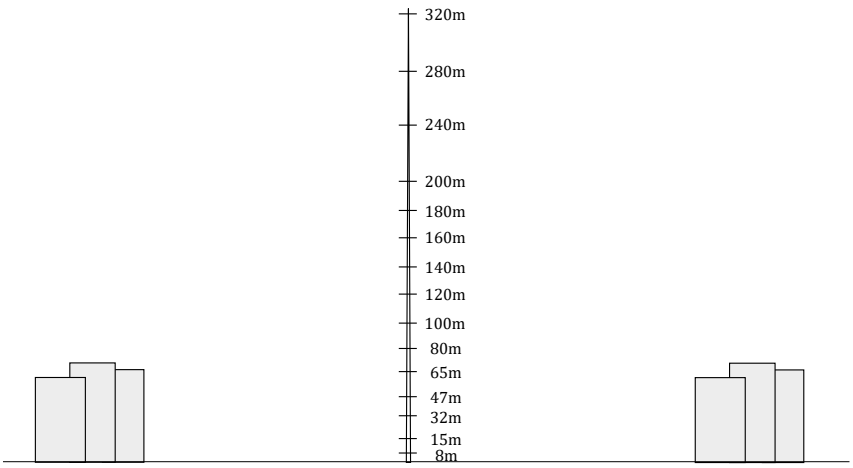

Figure 3 Sketch of the 325 m meteorological tower in Beijing, and the height of each observation platform at which meteorological parameters were measured.

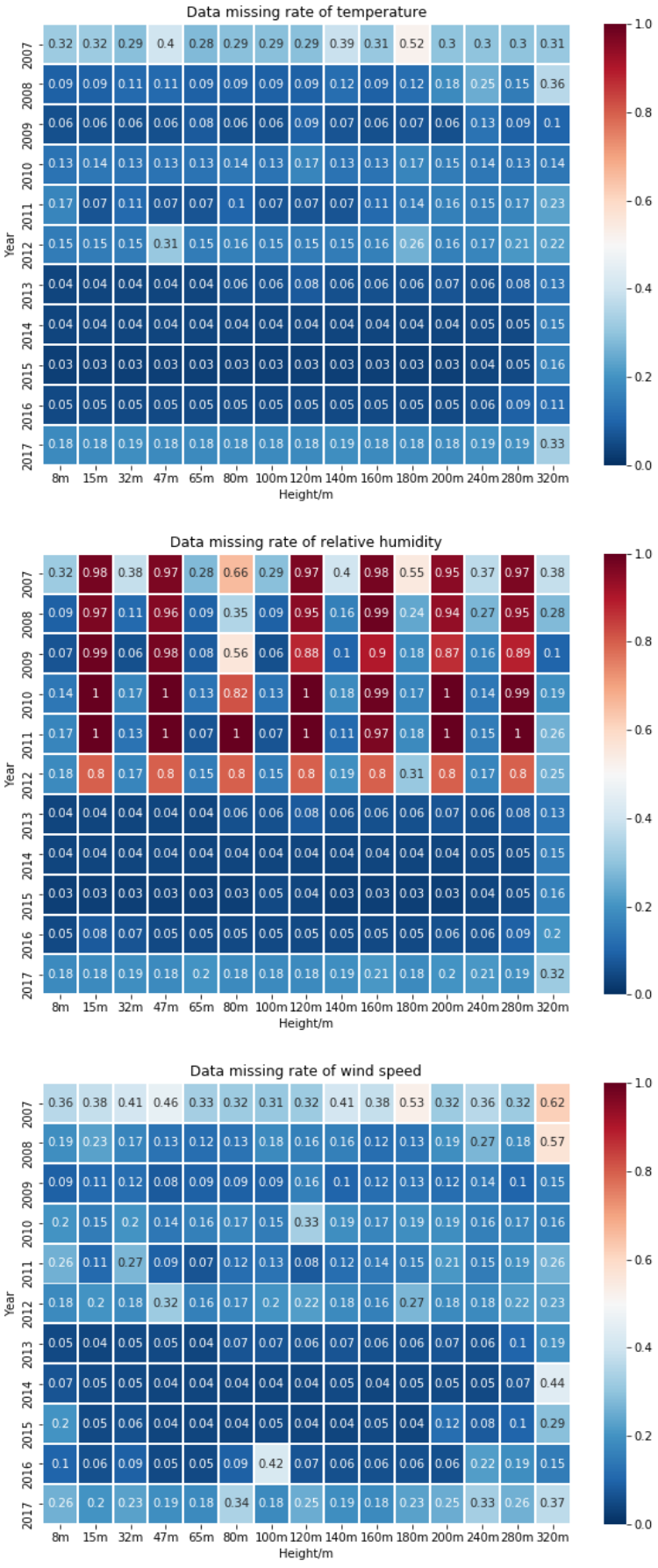

Figure 4 Missing rates of measured data from 2007 to 2018 (temperature, relative

humidity, wind speed).

2.2 Taller-building energy model

We used the Designer's Simulation Toolkit (DeST) software [24] to develop an energy model of tall buildings and run simulations to investigate the influence of the vertical variations of weather parameters on cooling and heating loads. DeST is a computational tool used for building environments and energy performance simulations. The residential building simulation module (DeST-h) and commercial building simulation module (DeST-c) are widely used in engineering and research in China to solve practical problems at different building life-cycle stages [25]. Users may modify meteorological parameter input files independently in DeST, which is the basis for implementing the simulation in this study.

The simulation model was developed based on a tall office building with a height of approximately 250 m in Beijing. The total building floor area is 106 000 m^2, and the area of a typical floor is 2200 m^2, with approximately 80% of this area (1790 m^2) being air-conditioned. A three-dimensional (3D) sketch and a typical floor plan are shown in Figure 5. The detailed input parameters were determined according to the actual building conditions, as shown in Table 1. The schedule of air-conditioning was determined based on working hours; this was from 7:00 to 21:00. The thermal parameters of the envelope were established in accordance with the latest national standard in China, the GB50189-2015 Design Standards for Energy Efficiency of Public Buildings [26], as shown in Table 2.

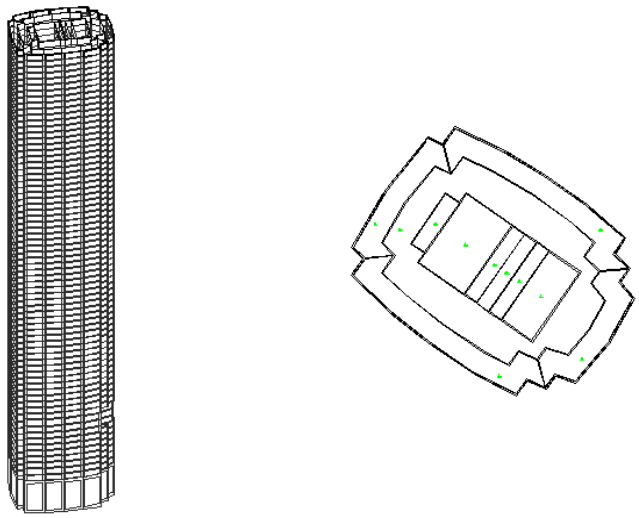

(a) 3D sketch of the model (b) Plan of a standard floor

Figure 5 Sketch of the tall-building simulation model developed in this study.

Table 1 Indoor environmental parameters of the tall-building simulation model.

	Summer		Winter		Fresh-air volume （m^3/h·person）
	Setpoint temperature （℃）	Relative humidity （%）	Setpoint temperature （℃）	Relative humidity （%）	
Lobby	25	55	16	—	16

Office	25	55	20	40	40

Table 2 Thermal parameters of building envelope.

Roof U-factor	0.453 W/m²·K
Non-transparent wall U-factor	0.498 W/m²·K
Transparent curtain wall U-factor and solar shading coefficient (SC)	1.9 W/m²·K
	SC：0.402 (non-North)/0.69 (North)

Because DeST employs a user-defined constant convective heat transfer coefficient to calculate the exterior-surface heat balance, we selected the annual average wind speed (V) at the height of the standard floor to calculate the convective coefficient (h_c) using equation (1) and (2) [27]. Because the wind speed in Beijing in winter is greater than in summer, this simplification will make the calculated cooling load larger and the heating load smaller. However, compared with the difference in wind speed at different heights, the difference in wind speed in different seasons is smaller, therefore, this simplification is reasonable overall.

$$h_C = 5.82 + 3.95V \quad \text{if } \mathrm{V} \leq 5\mathrm{m/s} \qquad (1)$$

$$h_c = 7.14V^{0.78} \quad \text{if } \mathrm{V} > 5\mathrm{m/s} \qquad (2)$$

Because DeST does not currently consider changes to weather variables along height, only one set of meteorological parameters at a certain height (usually at ground level) may be used as weather data input in each simulation. Therefore, to simulate and compare the cooling and heating loads of floors at different heights, we separately simulated building loads at different heights using the corresponding set of meteorological conditions. We used the results of the standard floor from each simulation for further analysis.

3 Vertical profiles of meteorological parameters.

3.1 Dry-bulb temperature

The hourly outdoor air dry-bulb temperature varies significantly with height. The frequency distribution of the dry-bulb temperature at various heights showed two peaks. For the 8-m-high observatory platform, the peaks were within 2 and 3 °C and 24 and 25 °C. For the 140 m platform, the peaks were within 0 and 1 °C and 23 and 24 °C. For the 320 m platform, the peaks were within –1 and 0 °C and 22 and 23 °C. As the height increases, the peak temperature decreases. Figure 6 shows the 24 h dry-bulb temperature curves on two typical summer days at different heights, and Figure 7 illustrates these curves on two typical winter days. The daily curves at different heights were observed to be similar. The difference between the dry-bulb temperature measured at the 8-m-high platform and the 320-m-high platform was approximately 4 °C at 16:00. The daily range of the 8 m platform was higher than that of the 320 m platform.

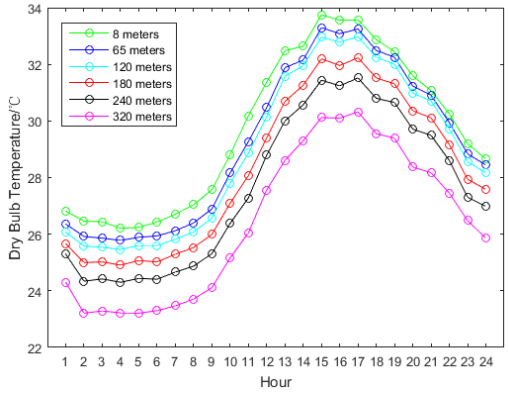

(a) 11th August, 2015

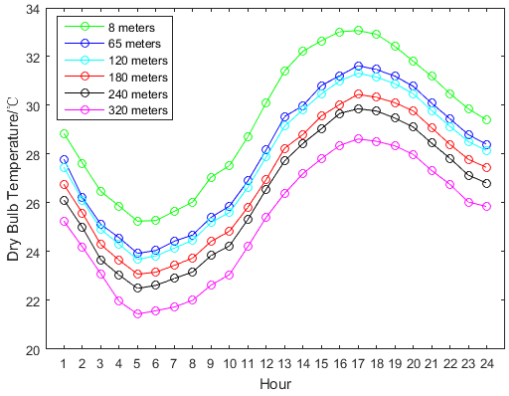

(b) 8th July, 2015

Figure 6 Dry-bulb temperature curves from 24 h observations on two typical summer days.

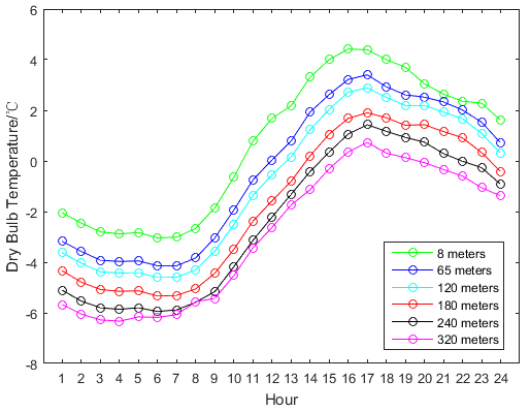

(a) 22nd February, 2015

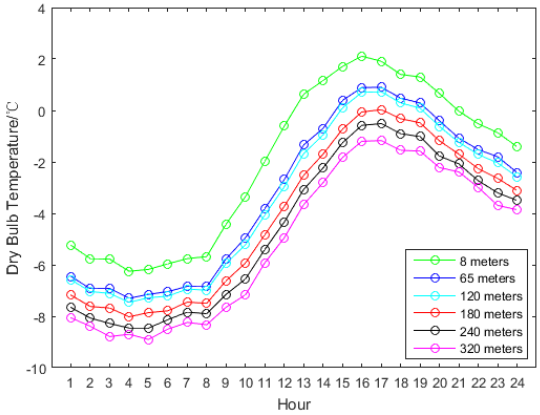

(b) 31st January, 2016

Figure 7 Dry-bulb temperature curves from 24 h observations on two typical winter days.

The average value and standard deviation of the measured dry-bulb temperature at different platforms on summer days is shown in Figure 8, and the same data is shown in Figure 9 for winter days. For winter and summer days, the dry-bulb temperature tends to decrease as the vertical height increases, with changes exhibiting a near-linear pattern, consistent with previous research findings [28, 29]. Changes were clearer at 12:00 and 18:00 than at 6:00 and 24:00. Quantitative analysis of the vertical temperature drop was performed by piecewise fitting using the data of two adjacent observatory platforms. Based on the statistics of 96 260 h of temperature data between 2007 and 2017, the temperature gradient was found to be 0.9 °C per 100 m.

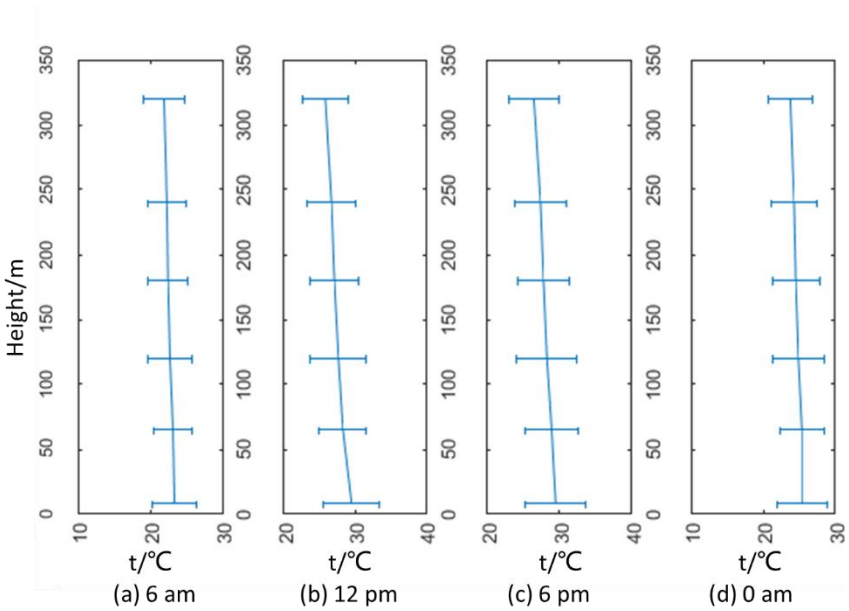

Figure 8 Average (±standard deviation) of dry-bulb temperature measured in June, July, and August from 2007 to 2017 at 6:00, 12:00, 18:00, and 24:00.

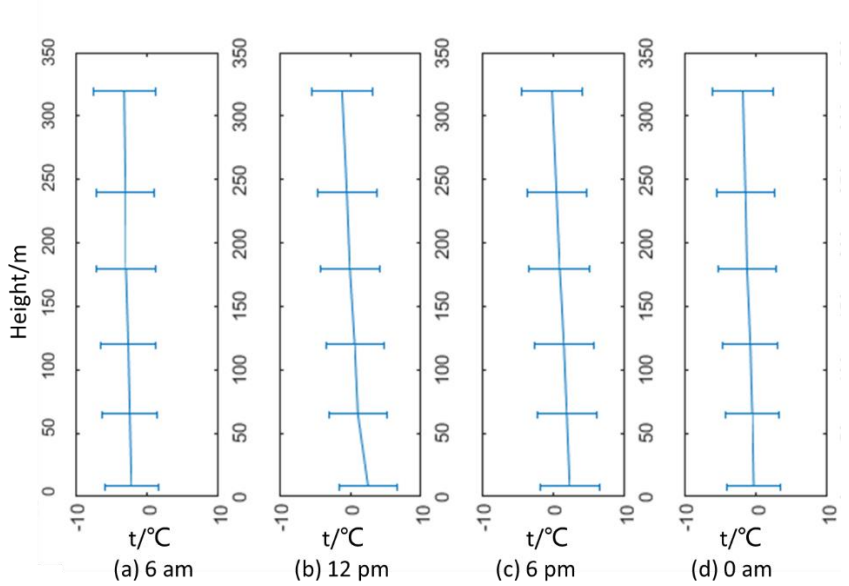

Figure 9 Average (±standard deviation) of dry-bulb temperature measured in January, February, and December from 2007 to 2017 at 6:00, 12:00, 18:00, and 24:00.

Temperature inversion, defined as the temperature increase with height, is a common phenomenon in the atmospheric boundary layer [30–33]. This phenomenon has also been observed in Beijing on some days. The probability of the temperature inversion phenomenon at each height segment was calculated, as shown in Figure 10. Each sub-figure is a frequency distribution of the temperature change per 100 m calculated between two platforms. The number of hours used to carry out the statistics and the probability of temperature inversion phenomenon are noted as ">0". This means that the temperature increases as the height increases. The probability of a temperature drop between a height of 8 and 32 m was high, at 35.31%.

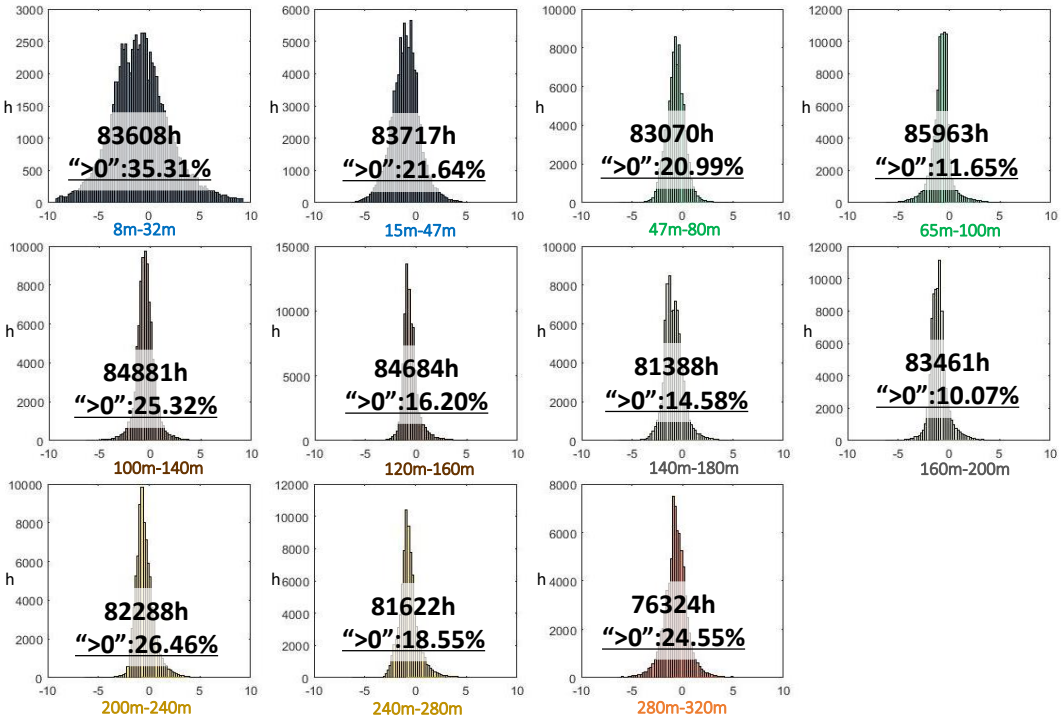

Figure 10 Frequency distribution of the vertical temperature gradient (represented as temperature change per 100 m) calculated between two adjacent platforms.

At different heights, there was a variance in the daily temperature range (i.e., maximum to minimum temperature). Figure 11 shows the average daily ranges at various heights, illustrating that with an increase in vertical height, the daily temperature range decreases. The average daily range of temperature at 320 m was approximately 2.50 °C less than at 8 m. The daily maximum and minimum temperatures at each altitude were also calculated, as listed in Table 3. The daily maximum temperature at each altitude occurs most frequently at 15:00 and 16:00, and the daily minimum temperature occurs most frequently at 6:00 and 7:00.

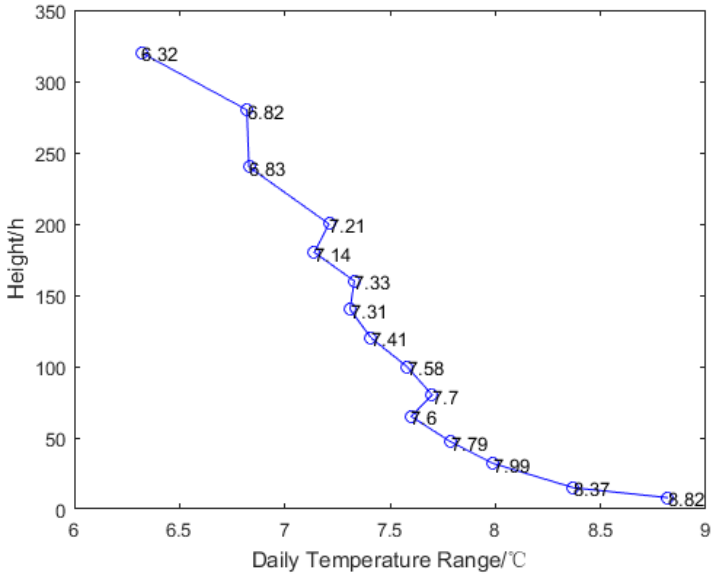

Figure 11 Variation of the daily temperature range with altitude.

Table 3 Most frequent times for the daily highest and lowest temperatures (statistics from 3416 d of data).

Height		8 m	32 m	65 m	80 m	120 m	160 m	200 m	240 m	280 m	320 m
Peak	Time	15:00	15:00	16:00	16:00	16:00	16:00	16:00	16:00	16:00	16:00
	Proportion	33%	28%	29%	29%	29%	26%	27%	26%	23%	23%
Valley	Time	6:00	6:00	6:00	6:00	7:00	6:00	7:00	7:00	7:00	7:00
	Proportion	28%	27%	26%	26%	24%	23%	20%	20%	18%	16%

3.2 Absolute humidity

Relative humidity is the ratio of the partial pressure of water vapor to the equilibrium vapor pressure of water at a given temperature, depending on the air dry-bulb temperature. Therefore, to study the vertical gradient of humidity independently, we chose to analyze absolute humidity, which is not influenced by dry-bulb temperature. The absolute humidity was calculated based on the measured relative humidity and dry-bulb temperature. Figure 12 shows the frequency distribution of hourly absolute humidity at different heights, where the unit is g/kg of dry air and the ordinate is the frequency. The absolute humidity frequency distribution curves at different heights were similar, where the most frequent values were between 0.7 and 0.9 g/kg of dry air, with no obvious change in the absolute humidity at different heights. The average and standard deviation of absolute humidity at different platforms on summer and winter days are shown in Figure 13 and Figure 14, respectively. The average did not vary considerably with height, with the main trend being humid in summer and dry in winter, which is a typical climate of Beijing. The average absolute humidity was approximately 1.5, and 15 g/kg of dry air in winter and summer, respectively.

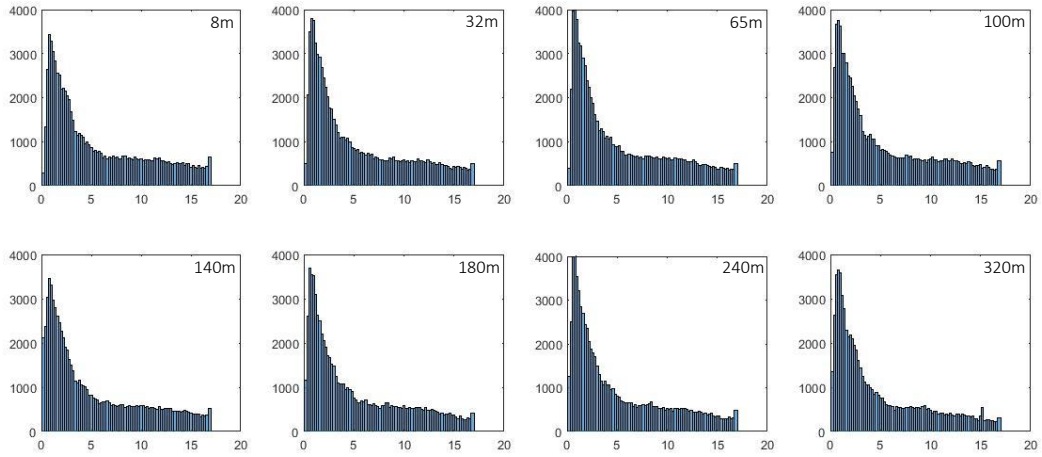

Fig. 12 Frequency distribution of outdoor air absolute humidity at different heights (vertical axis – count, horizontal axis – air absolute humidity in g/kg of dry air).

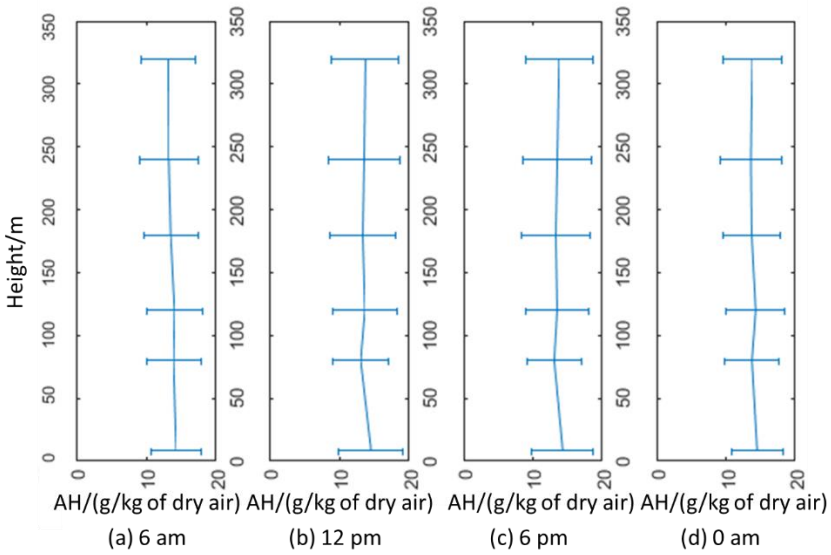

Figure 13 Average (±standard deviation) of absolute humidity in June, July, and August from 2007 to 2017 at 6:00, 12:00, 18:00, and 24:00.

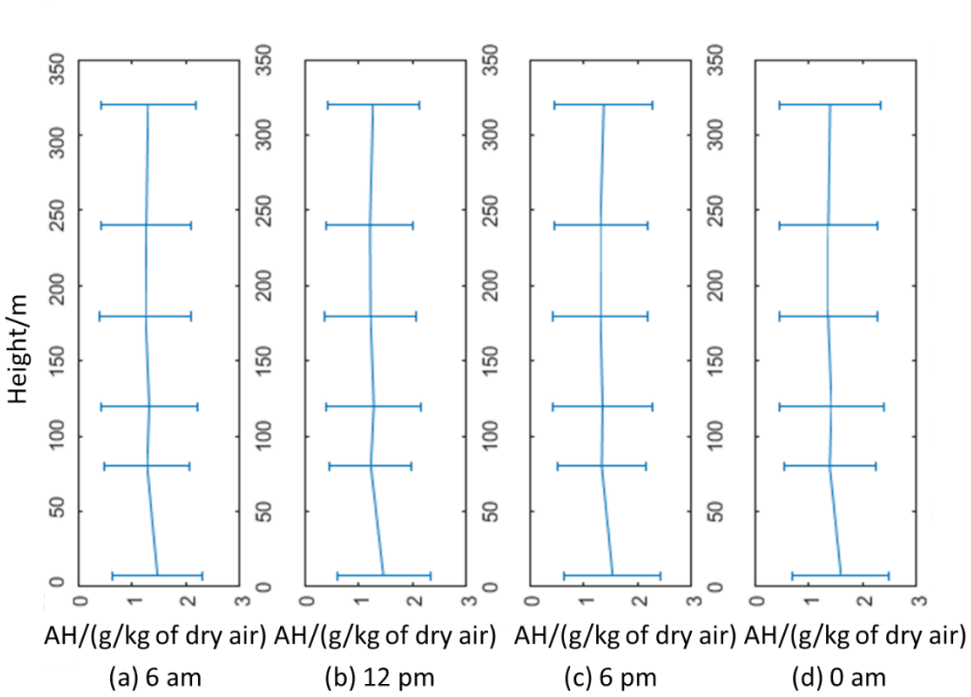

Figure 14 Average (±standard deviation) of absolute humidity in January, February, and December from 2007 to 2017 at 6:00, 12:00, 18:00, and 24:00.

3.3 Wind speed

The hourly measured wind speed at each altitude, from 8 m (ground) to 300 m, showed that the wind speed increases significantly with height. The distribution frequency statistics of hourly wind speed at each platform were calculated and are shown in Figure 15. As the height increases, the peak wind speed increases. The peak at the 8 m platform was between 1.2–1.4 m/s, while at the 240 m platform the range was 3.2–3.4 m/s. The average and standard deviation of the wind speed at different platforms on summer and winter days are shown in Figure 16 and Figure 17, respectively. The average wind speed as well as the standard deviation tends to increase with vertical height. As the height increases, the changing rate of wind speed also decreases, which is consistent with some previous research findings [34, 35]. Using the piecewise fitting from the data of two adjacent platforms based on the statistics of 96 360 h of wind-speed data, the wind speed was found to increase by 2 m/s per 100 m in most cases.

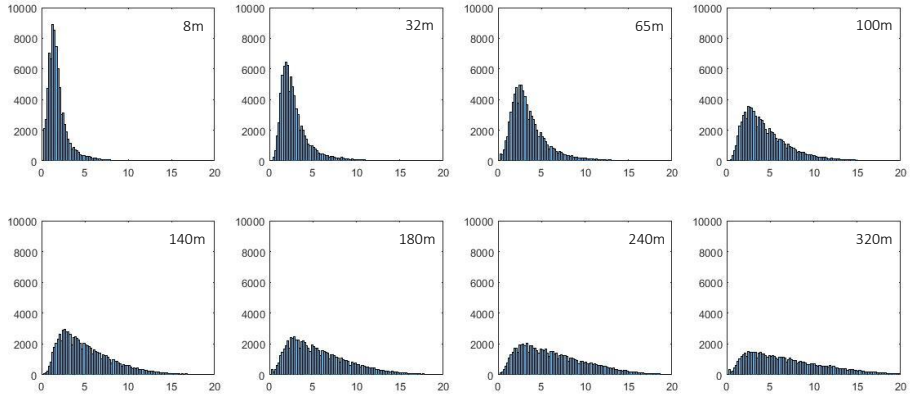

Figure 15 Frequency distribution of hourly wind speed (m/s) at different heights.

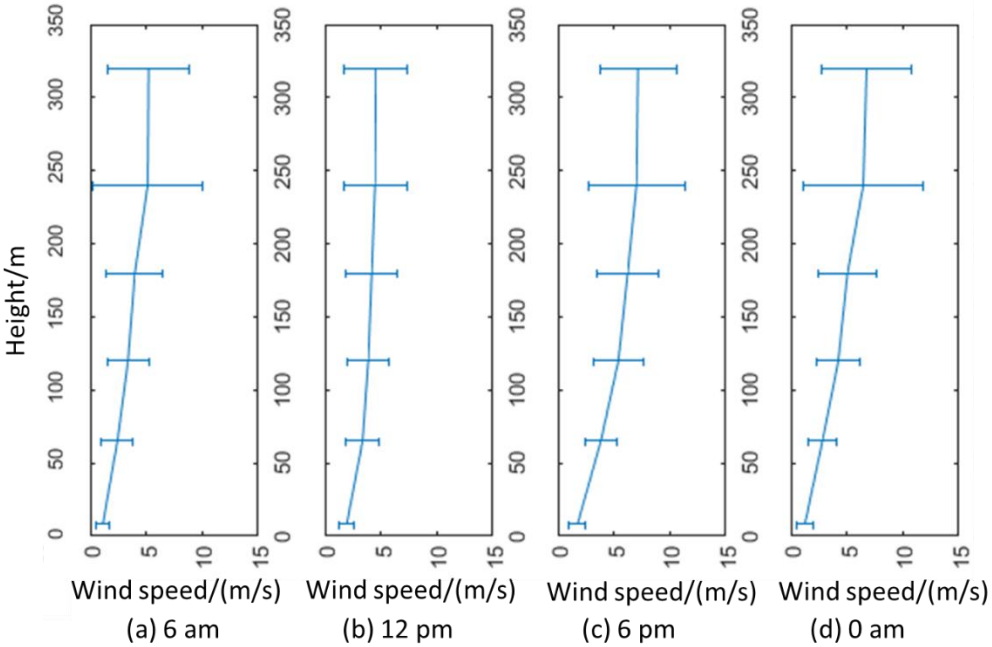

Figure 16 Average (±standard deviation) wind speed measured in June, July, and August from 2007 to 2017 at 6:00, 12:00, 18:00, and 24:00.

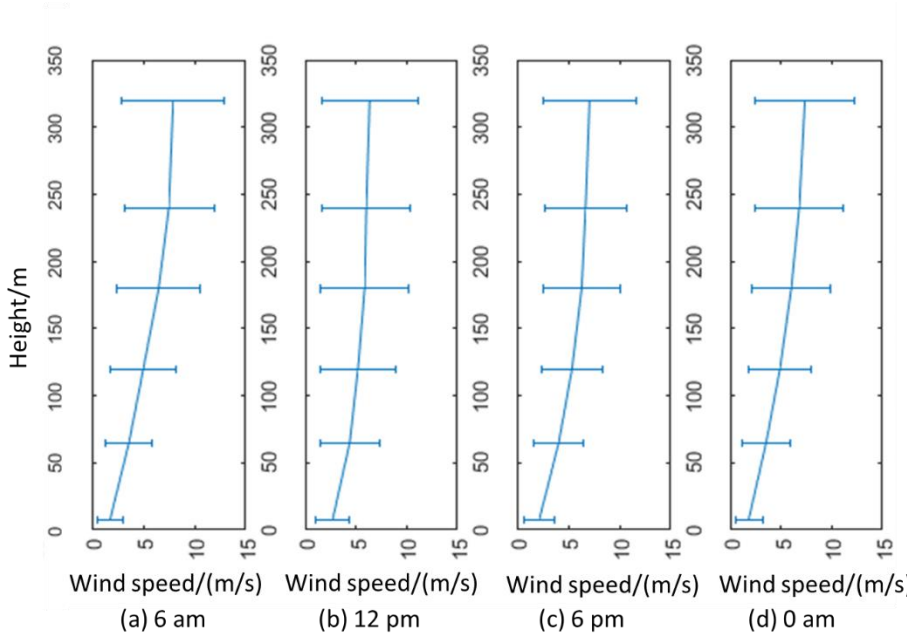

Figure 17 Average (±standard deviation) wind speed measured in January, February, and December from 2007 to 2017 at 6:00, 12:00, 18:00, and 24:00.

To further analyze the change at each height segment, Figure 18 shows the statistical results of changes in wind speed at each height. As height increases, the rate of change in wind speed decreases. At heights between 0 and 50 m, the wind speed increases by 3.71 m/s per 100 m. In contrast, at heights between 250 and 300 m, the wind speed increases by 0.59 m/s per 100 m, which is much less than the gradient under 50 m. No significant difference was found across months.

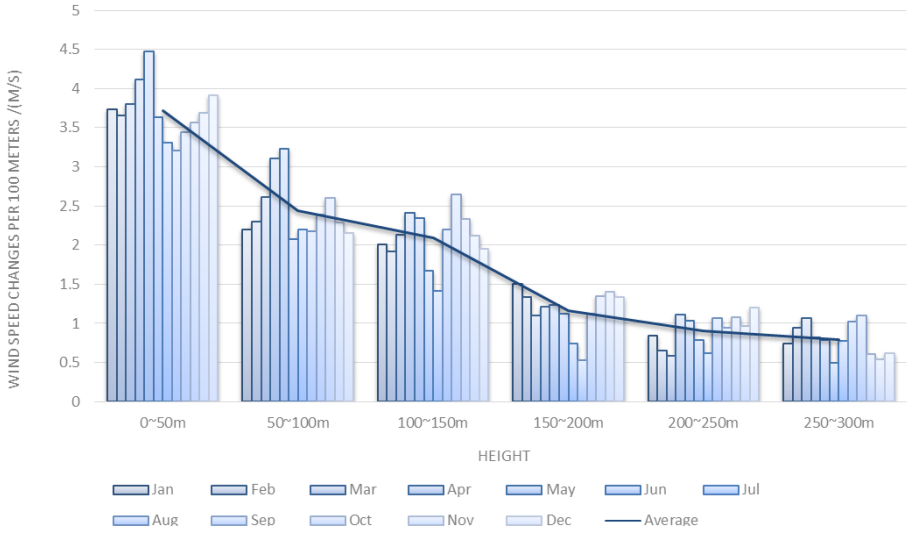

Figure 18 Average wind speed change in m/s per 100 m in each month.

3.4 Heating degree-day (HDD18) and cooling degree-day (CDD26)

The HDD and CDD at various heights were also calculated and analyzed. HDD is an indicator of heating demand during the heating season. HDD based on 18 °C (HDD18) and

CDD based on 26 °C (CDD26) were used in this study based on the national standard in China, "JGJ26 – 2010 Design Standard for Energy Efficiency of Residential Buildings in Severe Cold and Cold Zones." Equations (3) and (4) were used to calculate HDD18 and CDD26:

$$\mathrm{HDD18} = \sum_{d \in p,\ T_d < 18} (18 - T_d) \qquad (3)$$

$$\mathrm{CDD26} = \sum_{d \in p,\ T_d > 26} (T_d - 26) \qquad (4)$$

where T_d is the average dry-bulb temperature of day d, and p is the period in which HDD and CDD were calculated. In this study, each year was a statistical period.

Statistics on HDD18 and CDD26 from the observation data at each platform are shown in Figure 19. The HDD18 and CDD26 both change significantly with height; the HDD18 at a height of 320 m increased from that at 8 m by approximately 400 °C/ d, while the CDD26 at 320 m decreased from that at 8 m by approximately 400 °C/ d. This shows that the differences in CDD26 and HDD18 were similar. Among the different years, 2011 had the highest HDD18 with the coldest winter, while 2014 had the lowest HDD18 with the warmest winter. In terms of CDD26, the results of 2007, 2008, and 2012 were lower with a cooler summer, while 2014 and 2017 had higher results with a hotter summer.

(a) HDD18

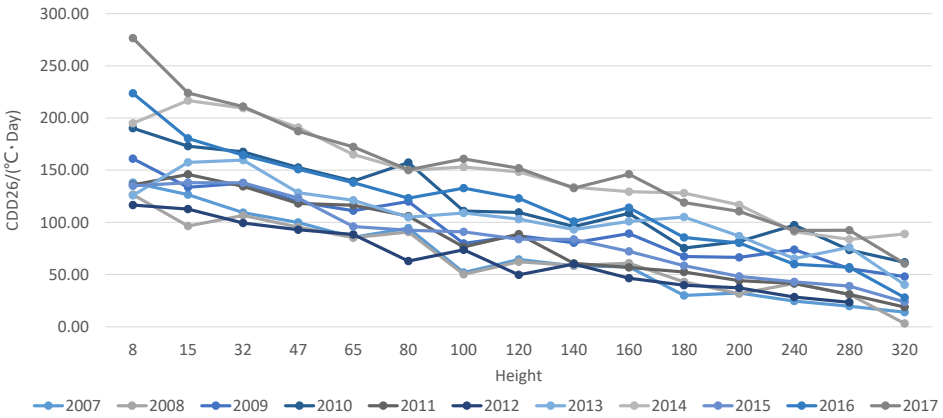

(b) CDD26

Figure 19 (a) HDD18 and (b) CDD26 at various heights in this study.

4 Heating and cooling loads at various heights

4.1 Loads at various heights

The hourly dry-bulb temperature, hourly absolute humidity, and annual average wind speed at each height were used as input meteorological parameters for the building performance simulation. The annual and peak loads at each height are shown in Figure 20. Variations in the heating load at different heights were clearer than the cooling load, and the variation in the annual load at different heights was clearer than the peak load.

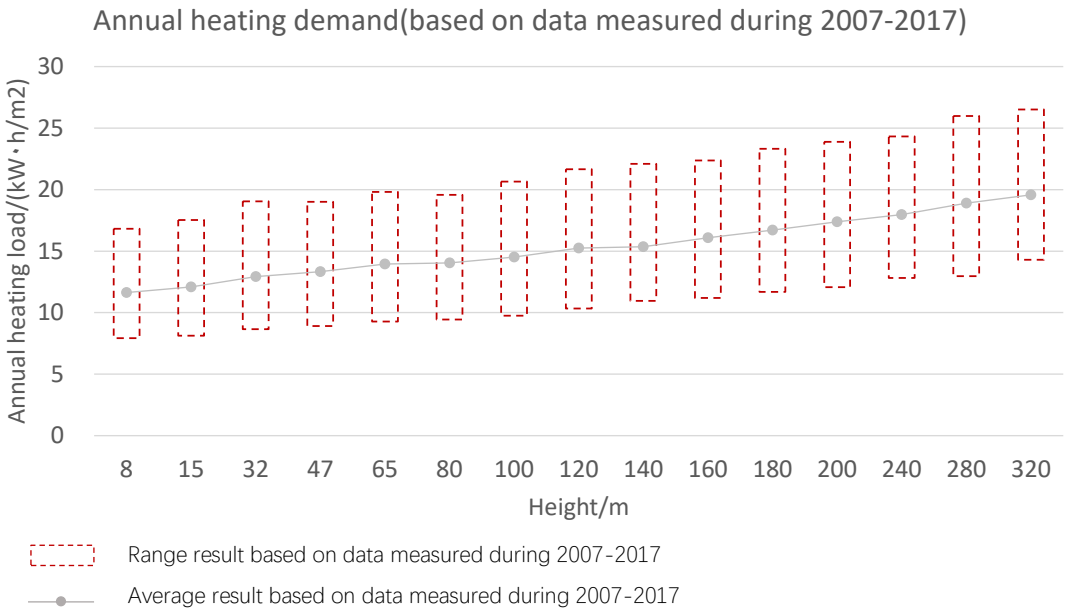

(a) Annual heating demand (based on data measured from 2007 to 2017).

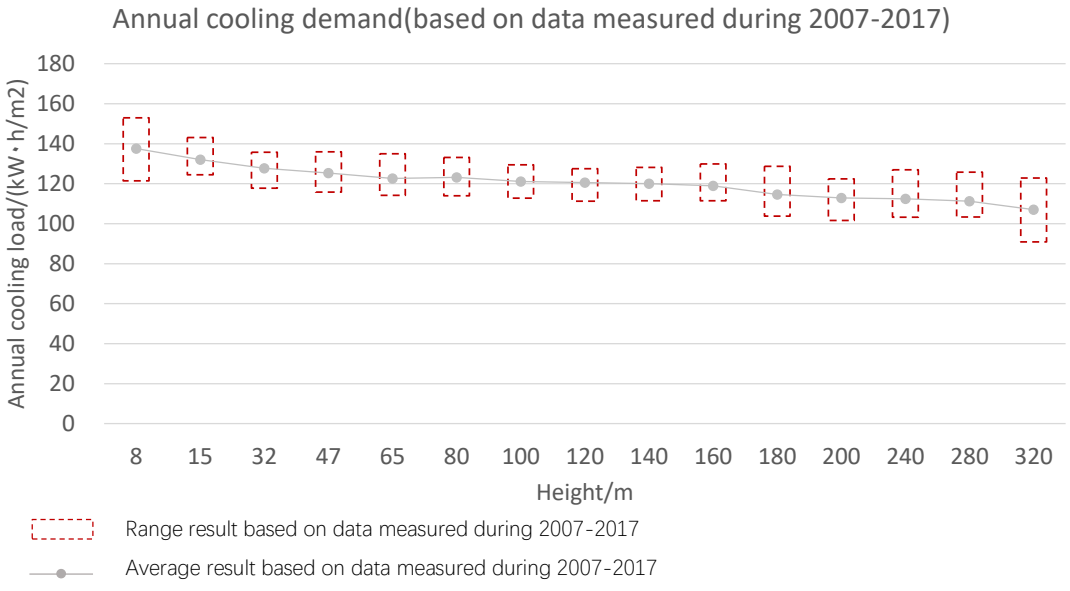

(b) Annual cooling demand (based on data measured from 2007 to 2017).

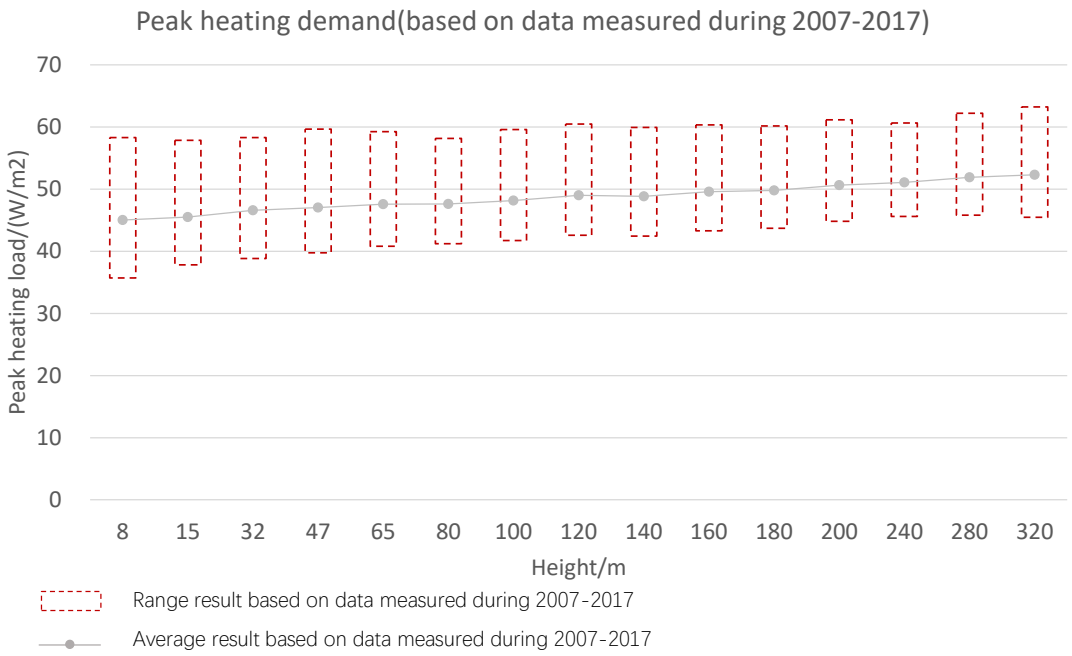

(c) Peak heating demand (based on data measured from 2007 to 2017).

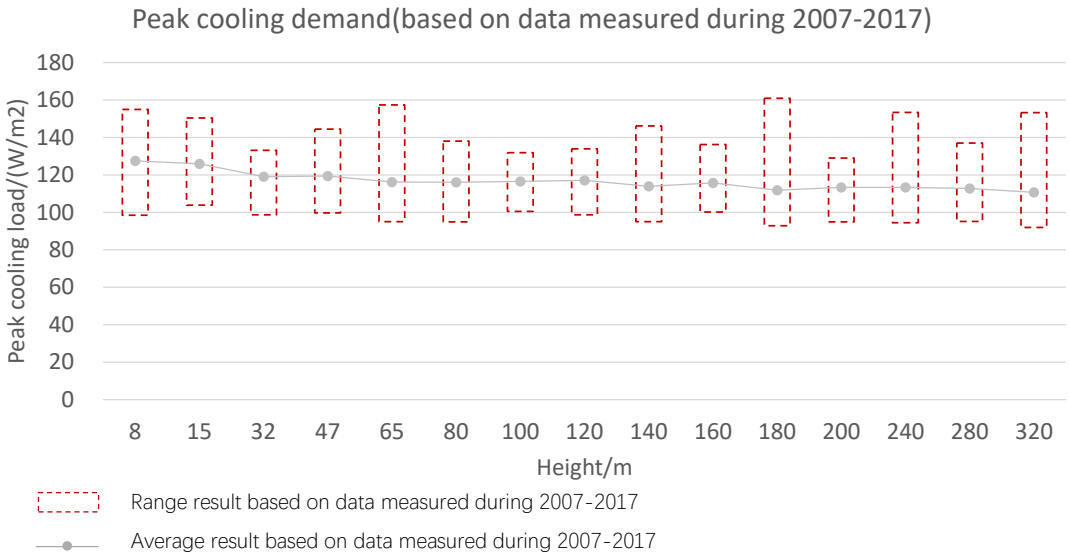

(d) Peak cooling demand (based on data measured from 2007 to 2017).

Figure 20 Heating and cooling demand at each height (based on data from 2007 to 2017).

The hourly load curve shows that under actual weather conditions, the hourly load significantly changes with increasing height, where the change in heating load with height is more distinctive. Figure 21 shows that the hourly load difference between the 8 and 320 m heights at 9:00 was approximately 30 W/m^2.

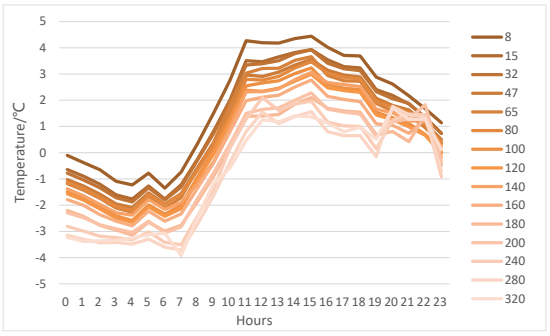

(a) Temperature Curve (2015-01-07)

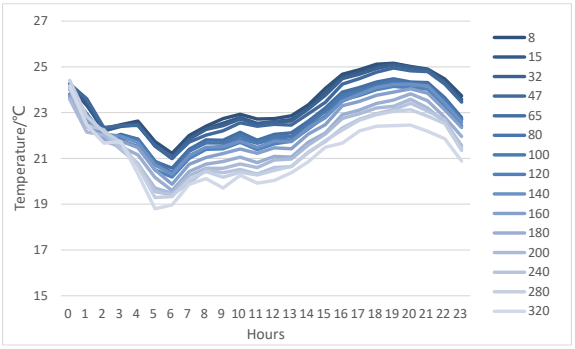

(b) Temperature Curve (2015-07-16)

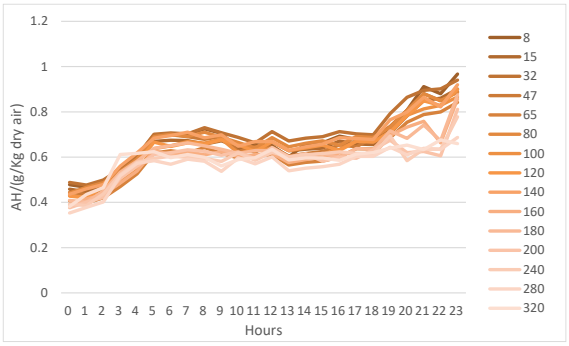

(c) Absolute Humidity Curve (2015-01-07)

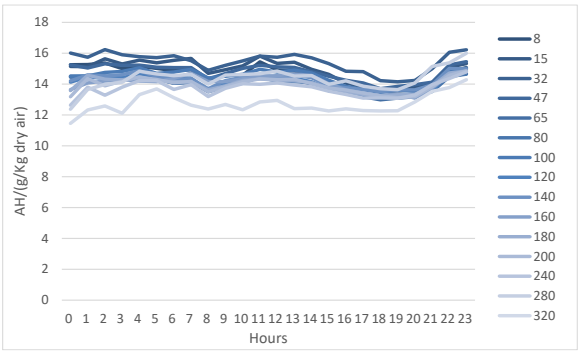

(d) Absolute Humidity Curve (2015-07-16)

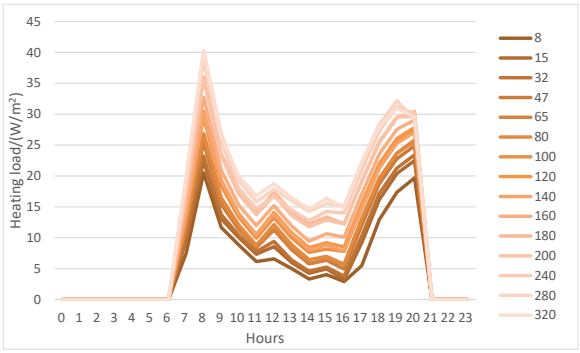

(e) Heating Load Curve (2015-01-07)

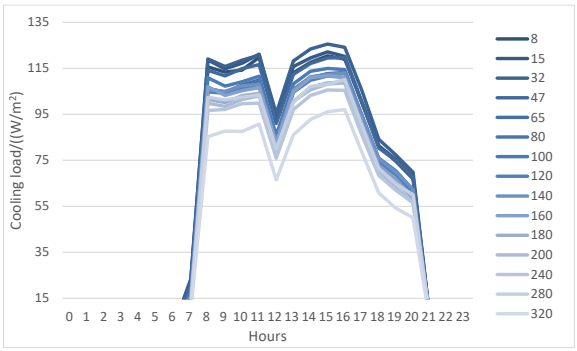

(f) Cooling Load Curve (2015-07-16)

Fig. 21 Load curves and the corresponding dry-bulb temperature and absolute humidity curves.

To compare loads at different heights, the annual heating and cooling loads based on the 2013–2016 meteorological data are shown in Figure 22. The ordinates in Figure 22 are the ratio of the annual cooling and heating loads at the corresponding height to the annual cooling and heating loads at 8 m. For each year, it was observed that the annual cooling load decreases with increasing height, while the annual heating load increases significantly with height; the change for the latter is more significant than the annual cooling load. The annual heating load at 320 m was approximately 85% more than the load at 8 m, and the annual cooling load at 320 m was approximately 20% less than the load at 8 m.

(a) Annual heating demand at X m / value at 8 m (b) Annual cooling demand at X m / value at 8 m

Fig. 22 Annual cooling and heating loads at different heights.

The peak load simulation results are shown in Figure 23, which illustrates that the peak load also changes with increasing height. The peak heating load increases with height, and the peak cooling load decreases with height, with the change in the former being more distinctive. The peak heating load at 320 m was approximately 20% more than the load at 8 m, and the peak cooling load at 320 m was approximately 10% less than the load at 8 m. Further comparison and analysis of the hourly heating loads show that the peak loads at different heights in each year often appeared at the same time. As the outdoor temperature tends to decrease with increasing height, the hourly heat load at this moment increases with height. It follows that the change in peak heating load with increasing height is mainly caused by the difference in the hourly temperature and the difference in wind speed.

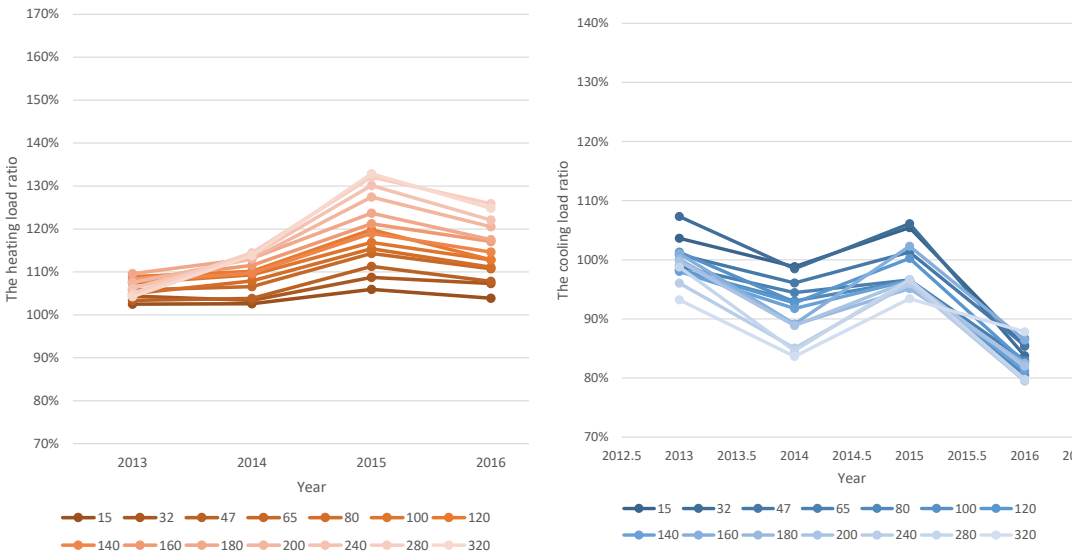

(a) Peak heating demand at X m / value at 8 m (b) Peak cooling demand at X m / value at 8 m

Fig. 23 Peak load simulation results at different heights.

4.2 Overall building thermal loads

Overall building thermal loads were calculated based on the simulation results of each floor using weather data at the corresponding height. Weather data at each height were not always available; therefore, we compared several scenarios of measurement heights and analyzed how they influenced the overall building heating and cooling loads, as shown in Table 4. The first scenario has only one measurement height at the ground level; therefore, the simulation results with the weather input at the ground level are representative of all floors of the building. The second scenario includes weather measurements at two heights: the ground and the top floor (roof) levels. The simulation results with the weather input at each measurement height represent half of the floors of the building. In general, for a building with weather measurements at n heights in addition to the ground and the top/roof (n ≥1), the building load is calculated using Equation (3):

$$Load_{all} = \frac{1}{2(n+1)} Load_{top} + \frac{1}{2(n+1)} Load_{ground} + \frac{1}{n+1} \sum_{k=1}^{n} Load_k \qquad (3)$$

where $Load_{top}$ is the simulated load using the weather data at the top floor/roof, $Load_{ground}$ is the simulated load using the weather data at the ground level, and $Load_k$ is the simulated load using the weather data measured at the k^{th} height. The simulation results of a 320 m building are shown in Table 4. The load ratio was defined as the ratio of the simulated loads of each scenario to the simulation loads of the 9-point measurement scenario shown in the last column of Table 4.

It is clear that a greater number of measurement heights improves the accuracy of the results. If only weather data at the ground level is used, the heating load ratio is 61.90%, which means an underestimation of 38.1%. Two height measurements can improve the heating load ratio to 94.52%. Therefore, it is crucial to obtain weather measurements at a minimum of two heights, if it is not possible to acquire more.

For the cooling load simulation, the weather measurements at the ground and top floor levels were adequate. However, using only ground-level weather data in the simulation will lead to an overestimation of 12.44% for the annual cooling load. To design and simulate high-rise buildings at different locations, measuring larger meteorological data points along the height is necessary. For the simulation of a high-rise building, if there is only one height level of meteorological data, it will lead to a relatively large error in the results, and if there are two measuring points at the ground and top-floor level, the accuracy of the results will be significantly improved.

Table 4 The simulated loads at different weather measurement scenarios.

Weather measurement scenarios							

Number of measurement heights	1 (Ground level)	2 (Ground and top-floor levels)	3	4	5	7	9
Annual cooling load (kW·h/m^2)	229290.0	204623.4	207084.2	203425.7	202183.4	204140.6	203929.2
Cooling load ratio	112.4%	100.3%	101.6%	99.8%	99.3%	100.1%	100.0%
Annual heating load (kW·h/m^2)	14594.4	22284.1	22034.1	23301.8	23399.8	23330.3	23575.5
Heating load ratio	61.9%	94.5%	93.5%	98.8%	99.6%	99.0%	100.0%

5 Discussion

There are limited studies on the vertical profile of outdoor air temperature, humidity, and wind speed. Monin and Obukhov [36–39] first proposed their similarity theory in 1946, and several studies used related concepts for experiments and the derivation of the profile formula. These profiles were based on atmospheric stability in the atmospheric boundary layer. However, parameters of atmospheric stability are not easy to obtain in most cases, leading to difficulties in generating meteorological profiles. The current study demonstrates more general vertical meteorological patterns.

As this study is based on data measured for the 325 m Tower in Beijing, the results and findings may be applied to the Beijing area. The surface characteristics of tall buildings differ between locations, which affect the vertical pattern; therefore, the applicability of these results to other geographic areas requires more measured data for verification. There are some studies on vertical meteorological patterns based on measured data from other regions. Cao [40] analyzed the measured temperature data of the 255-m-high Tianjin Meteorological Tower and found that the temperature decreased by 1.1 °C every 100 m along the vertical direction. Leung [41] monitored the temperature and humidity of an approximately 300-m-high building in downtown Chicago for a week and calculated the averages for each height. The temperature decreased by 0.56 °C every 100 m, similar to the commonly used standard lapse rate of –0.65 °C per 100 m. The absolute humidity showed no obvious changes across various heights. Song et al. [13, 14] presented the monthly averages of temperature, humidity, and wind speed for different altitude groups. Between the lower two groups, the temperature drop is between 0.4 °C and 1.4 ℃ in different months, whereas the wind speed increases in the range of 0.7 m/s and 1.9 m/s. Most of the temperature drops in their measurement data were greater than the standard value of 0.65 °C, however, there was no significant difference in absolute humidity at different heights. In the case of limited vertical meteorological measured data, the pattern of the current study can be used as a reference for simulations in other regions, but vertical meteorological data from different regions would in improving the accuracy of the pattern.

In addition, the measured data used in this study were collected from an unobstructed meteorological tower, therefore the influence of the obstruction of the surrounding buildings

was not considered. In actual situations, high-rise buildings are often situated in a group of buildings that may in turn be affected by other surroundings. The surroundings of a high-rise have a greater impact on the lower floors than on the higher floors. Owing to the shading of the building, the outdoor wind speed and solar radiation on the lower floors will change, which may cause the vertical meteorological patterns to change. Lu et al. [42] and Tong et al. [43] analyzed the influence of the surroundings on the microclimate outside the building. The complexity of the surroundings reduces the wind speed. Occlusion of surrounding buildings will reduce solar radiation at several moments. The decrease in wind speed will result in a decrease in the cooling and heating loads of the lower floors, and the decrease in solar radiation will lead to a decrease in the cooling load of the lower floors and an increase in the heating load. In general, the influence of the surroundings will lead to a reduction in the cooling load of the lower floors, weakening the difference in cooling load of different floors. However, to determine the influence of the surroundings on heating load, it is necessary to comprehensively investigate the influence of wind speed and solar radiation.

6 Conclusions

This study analyzed the vertical meteorological gradients in Beijing based on 11 years of hourly outdoor air dry-bulb temperature, relative humidity, and wind speed measured at 15 observation platforms at a 325 m meteorological tower in Beijing. The results show that the hourly dry-bulb temperature decreases significantly with increasing altitude by approximately 0.9 °C per 100 m. The daily temperature difference decreases with increasing altitude, and temperature inversion has also been observed in Beijing on some days. The probability of a temperature drop between 8 and 32 m heights was high, at 35.31%. However, the absolute humidity remains almost the same at every level. As altitude increases, the wind speed increases significantly by approximately 2 m/s per 100 m; however, the rate of change in wind speed decreases. On an annual basis, the HDD18 at 320 m increases by 400 °C/ d from that at 8 m. The CDD26 at 320 m decreases by approximately the same magnitude from 8 m.

To investigate the impact of vertical weather gradients on the building cooling and heating loads, we conducted a building performance simulation of a tall building using DeST. The simulation results show that the annual cooling and heating loads vary with height. The influence of height on the heating load was more significant than the cooling load. The annual heating load increases with height, while the annual cooling load decreases with increasing height. The annual heating load at 320 m height was approximately 85% more than that at 8 m. In contrast, the annual cooling load was approximately 20% less than that at 8 m. At 320 m, the peak heating and cooling loads were approximately 120% and 90% of the value at 8 m, respectively. This demonstrates that the impact of vertical meteorological gradients should be considered for a 300-m tall building. The difference in the building cooling and heating loads across different heights was mainly due to vertical temperature differences. Although the effect of wind speed differences on thermal loads was lower than that of dry-bulb temperature, it cannot be negated. The peak heating load also increases significantly with height, mainly due to differences in hourly temperature and wind speed.

We recommended that weather measurements be taken for at least the ground and top

floor levels to ensure the accuracy of simulation results for tall buildings. Findings of vertical meteorological gradients and requirements of weather data for tall buildings can inform the design and operation of tall buildings.

It would be beneficial in future research to investigate similar meteorological tower data in different climatic regions to identify change in patterns and the extent of these changes. There is also a need to develop a methodology to generate weather data at various heights from measurements taken at the ground level, as most cities may not have weather data from meteorological towers; however, this does not negate the need to support the design of tall buildings in these cities.

Acknowledgements

This study was supported by "the 13th Five-Year" National Science and Technology Major Project of China (No. 2018YFC0704500), Beijing Municipal Natural Science Foundation of China (Grant number 8182026), the National Natural Science Foundation of China (Grant No. 51708324), and "the 13th Five-Year" National Science and Technology Major Project of China (No. 2018YFE0196000),. The authors would also like to acknowledge the support from the Beijing Advanced Innovation Center for Future Urban Design, Beijing University of Civil Engineering and Architecture.

References

1. (CTBUH), T.C.o.T.B.a.U.H. *CTBUH Height Criteria for Measuring & Defining Tall Buildings* https://www.ctbuh.org/resource/height.
2. Development, M.o.H.a.U.-R., *GB 50352-2005 Uniform standard for design of civil buildings (in Chinese)*. 2019, China Architecture & Building Press.
3. (CTBUH), T.C.o.T.B.a.U.H. *The Skyscraper Center- Global Tall Building Database of the CYBUH* https://www.skyscrapercenter.com/.
4. Yoshino, H., T. Hong, and N. Nord, *IEA EBC annex 53: Total energy use in buildings—Analysis and evaluation methods*. Energy and Buildings, 2017. **152**: p. 124-136.
5. Herrera, M., et al., *A review of current and future weather data for building simulation.* Building Services Engineering Research and Technology, 2017. **38**(5): p. 602-627.
6. Wang, R., et al., *Some Meteorological parameteres related to heating and conditioning of tall building (in Chinese).* Meteorology, 1999(01): p. 40-43.
7. Tong, Z., Y. Chen, and A. Malkawi, *Estimating natural ventilation potential for high-rise buildings considering boundary layer meteorology.* Applied Energy, 2017. **193**: p. 276-286.
8. Chen, Y., Z. Tong, and A. Malkawi, *Investigating natural ventilation potentials across the globe: Regional and climatic variations.* Building and Environment, 2017. **122**: p. 386-396.
9. Jung, M., et al., *Weather-Delay Simulation Model Based on Vertical Weather Profile for High-Rise Building Construction.* Journal of Construction Engineering and Management, 2016. **142**(6): p. 04016007.

10. Saroglou, T., et al., *Towards energy efficient skyscrapers.* Energy and Buildings, 2017. **149**: p. 437-449.

11. SINHA, S., S.J. KUMAR, and N. KUMAR, *Energy conservation in high-rise buildings Changes in air conditioning load induced by vertical temperature and humidity profile in Delhi.* Energy Conversion and Management, 1988.

12. Segal, M., R. Turner, and D.T. a, *Using radiosonde meteorological data to better assess air conditioning loads in tall buildings.* Energy and Buildings, 2000. **31**(3): p. 243-250.

13. Song, D. and Y.S. Kim. *Heating and cooling load analysis of supertall building considering the vertical micro climate change*. in *CTBUH 2011 World Conference*. 2011. Seoul, KOREA.

14. Song, D. and Y.S. Kim, *Effects of vertical meteorological changes on heating and cooling loads of super tall buildings.* International Journal of High-Rise Buildings, 2012. **1**: p. 81-85.

15. Cao, J., *RESEARCH ON THE AIR CONDITIONING LOAD AND WIND & THERMAL PRESSURE IN MEGATALL BUILDING IN COLD REGION (in Chinese)*. 2017, Harbin Institute of Technology.

16. Zhang, C., *Research on the vertical distribution of air-conditioning load in a thousand-meter scale megatall building (in Chinese)*. 2013, Harbin Institute of Technology.

17. de la Paz, D., R. Borge, and A. Martilli, *Assessment of a high resolution annual WRF-BEP/CMAQ simulation for the urban area of Madrid (Spain).* Atmospheric Environment, 2016. **144**: p. 282-296.

18. Ellis, P.G. and P.A. Torcellini, *Simulating Tall Buildings Using EnergyPlus*, in *Ninth International Building Performance Simulation Association (IBPSA) Conference and Exhibition (Building Simulation 2005)* 2005: Montreal, Quebec

19. Crawley, D., et al. *Energyplus: An update*. in *SimBuild 2004, IBPSA-USA National Conference*. 2004. Boulder, CO, USA.

20. Peng, Z., *Statistical Analysis of Observation Data of 325m Meteorological Tower in Beijing (in Chinese)*. 2005, Institute of Atmospheric Physics, Chinese Academy of Sciences.

21. Development, M.o.H.a.U.-R., *JGJ 26-2010 Design standard for energy efficiency of residential buildings in severe cold and cold zones (in Chinese)*. 2010, China Architecture & Building Press. p. 175P.;B5.

22. (ECMWF), T.E.C.f.M.-R.W.F. *ECMWF ERA5 Reanalysis* https://www.ecmwf.int/en/forecasts/datasets/reanalysis-datasets/era5.

23. Liu, S. and Y. Huang, *Discussion on effective sky temperature (in Chinese).* ACTA ENERGIAE SOLARIS SINIGA, 1983. **4**(1): p. 63-68.

24. Yan, D., et al., *DeST — An integrated building simulation toolkit Part I: Fundamentals.* Building Simulation, 2008. **1**(2): p. 95-110.

25. Zhu, D., et al., *A detailed loads comparison of three building energy modeling programs: EnergyPlus, DeST and DOE-2.1E.* Building Simulation, 2013. **6**(3): p. 323-335.

26. Development, M.o.H.a.U.-R., *GB 50189-2015 Design Standards for Energy Efficiency of Public Buildings*. 2015, China Architecture & Building Press. p. 89p:A4.

27. Liu, T., *Air conditioning design for super high-rise buildings (in Chinese)*. 2004:

China Construction Industry Press.

28. Lutgens, F.K., et al., *The Atmosphere: An Introduction to Meteorology*. 1982: Prentice Hall.

29. Foken, T., *Micrometeorology*. 2008, Berlin: Springer.

30. Kahl, J.D., *Characteristics of the low-level temperature inversion along the Alaskan Arctic coast.* International Journal of Climatology, 1990. **10**(5): p. 537-548.

31. Wolf, T., I. Esau, and J. Reuder, *Analysis of the vertical temperature structure in the Bergen valley, Norway, and its connection to pollution episodes.* Journal of Geophysical Research: Atmospheres, 2014. **119**(18): p. 10,645-10,662.

32. Ji, D., et al., *Analysis of heavy pollution episodes in selected cities of northern China.* Atmospheric Environment, 2012. **50**: p. 338-348.

33. Trompetter, W.J., et al., *Vertical and temporal variations of black carbon in New Zealand urban areas during winter.* Atmospheric Environment, 2013. **75**: p. 179-187.

34. Hsua, S.A., E.A. Meindlb, and D.B. Gilhousen, *Determining the Power-Law Wind-Profile Exponent under Near-Neutral Stability Conditions at Sea.* Journal of Applied Meteorology, 1994. **33**(6): p. 757-765.

35. Simmonds, P., *ASHRAE Design Guide for Tall, Supertall, and Megatall Building Systems*. 2015, ASHRAE: Atlanta, GA, USA.

36. Foken, T., *50 Years of the Monin–Obukhov Similarity Theory.* Boundary-Layer Meteorology, 2006. **119**(3): p. 431-447.

37. BUSINGER, J.A., et al., *Flux-Profile Relationships in the Atmospheric Surface Layer.* JOURNAL OF THE ATMOSPHERIC SCIENCES, 1971. **28**: p. 181-189.

38. Zilitinkevich, S.S., et al., *The Effect of Stratification on the Aerodynamic Roughness Length and Displacement Height.* Boundary-Layer Meteorology, 2008. **129**(2): p. 179-190.

39. Pahlow, M., M.B. Parlange, and F. Porté-Agel, *On Monin–Obukhov Similarity In The Stable Atmospheric Boundary Layer.* Boundary-Layer Meteorology, 2001: p. 225-248.

40. Cao, J., et al., *Assessment on meteorological parameters designed for the Heating, Ventilation and Air Conditioning (HVAC) systems in super high-rise buildings in Tianjin (Chinese).* Journal of Meteorology and Environment, 2019. **35**(4): p. 133-138.

41. Leung, L., P. Azimi, and B. Stephens, *How Do Outdoor Pollutant Concentrations Vary Along the Height of a Tall Building.* CTBUH Journal 2019 Issue I, 2019(1): p. 26-32.

42. Lu, J., et al., *High-Rise Buildings versus Outdoor Thermal Environment in Chongqing.* Sensors, 2007. **7**: p. 2183-2220.

43. Tong, Z., Y. Chen, and A. Malkawi, *Defining the Influence Region in neighborhood-scale CFD simulations for natural ventilation design.* Applied Energy, 2016. **182**: p. 625-633.